Supplementary Materials for

N^6-methyladenosine modification enables viral RNA to escape recognition by RNA sensor RIG-I

Mijia Lu[1¶], Zijie Zhang[2¶], Miaoge Xue[1], Boxuan Simen Zhao[2], Olivia Harder[1], Anzhong Li[1], Xueya Liang[1], Thomas Z. Gao[1], Yunsheng Xu[3], Jiyong Zhou[4], Zongdi Feng[5,6], Stefan Niewiesk[1], Mark E. Peeples[5,6], Chuan He[2,7], Jianrong Li[1]*

* Corresponding author: li.926@osu.edu

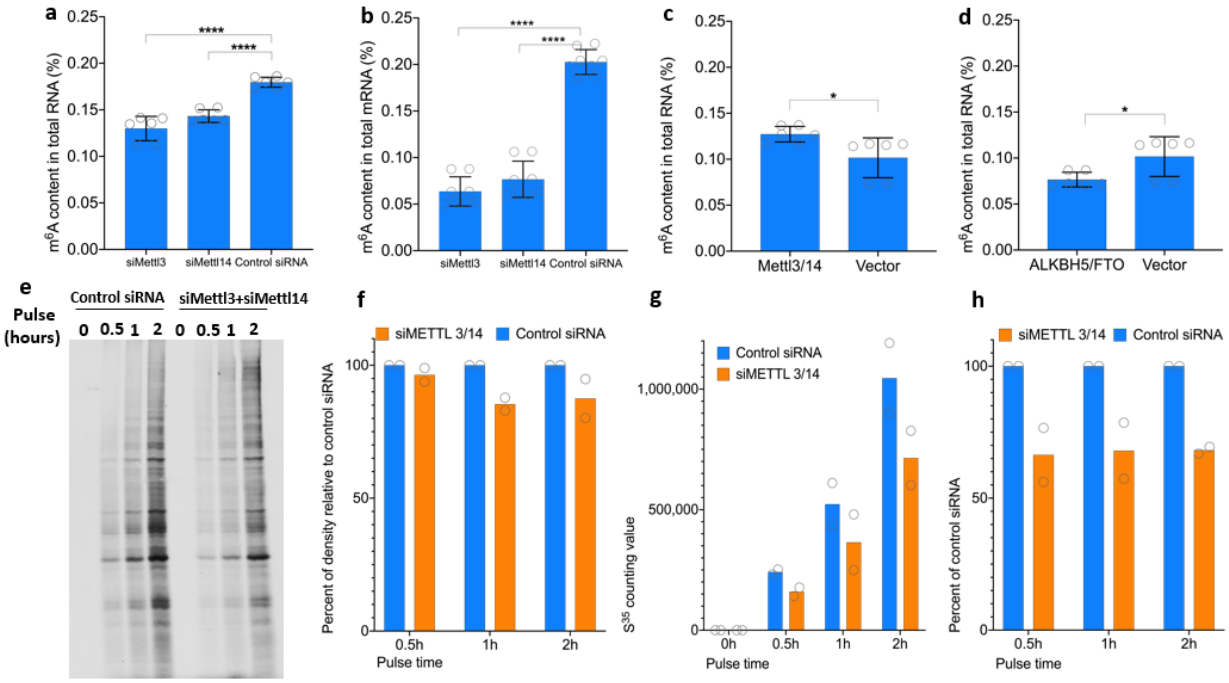

Supplementary Fig.1. The effects of writer and eraser proteins on host RNA m^{6}A methylation and host mRNA translation. (a) The effects of knockdown of writer proteins on total host RNA. A549 cells were transfected with siRNA targeting METTL3 and METTL14 or control siRNA. At 24 h post-transfection, total RNA was extracted from these cells. The m^{6}A level was quantified by m^{6}A RNA Methylation Assay Kit. **(b) The effects of knockdown of writer proteins on host mRNA.** Polyadenylated mRNA from panel A was isolated using poly-A beads, and m^{6}A level was quantified by m^{6}A RNA Methylation Assay Kit. **(c) The effects of overexpression of writer proteins on host RNA.** A549 cells were transfected with plasmids encoding METTL3 and METTL14 or control vector. At 24 h post-transfection, total RNA was extracted from these cells. The m^{6}A level was quantified by m^{6}A RNA Methylation Assay Kit**. (d) The effects of overexpression of eraser proteins on host RNA.** A549 cells were transfected with plasmids encoding FTO and ALKBH5 or control vector. At 24 h post-transfection, total RNA was extracted from these cells. The m^{6}A level was quantified by m^{6}A RNA Methylation Assay Kit**. (e) The effects of knockdown of writer proteins on host protein translation.** A549 cells were transfected with siRNA against METTL3 and METTL14 or control siRNA. After 24 h, cells were incubated in methionine- and cysteine-free media for 1 h, and 50 µCi of [^{35}S]-methionine was added. At 0.5, 1, 2 h, cells were washed with PBS, lysed in lysis buffer, analyzed by SDS-PAGE and exposed to film. **(f) Quantification of protein bands.** Quantification of protein bands in panel E was done using ImageJ software. **(g) [^{35}S] incorporation by scintillation counting.** 5 µl of each sample from panel E was used for measuring [^{35}S] incorporation by scintillation counting. **(h) Percent of [^{35}S] incorporation relative to control siRNA.** Percentage was calculated from panel **g**. Results are the means of $n = 3$ (**a, c, and d**) or $n = 4$ (**b**) biologically independent experiments ± standard deviation. The SDS-PAGE gel (**e**) is the representative of $n = 2$ biologically independent experiments. Results in panels **f, g, and h** are the means of $n = 2$ biologically independent experiments. Statistical significance was determined by two-sided student's *t*-test. Exact *P* values are included in Data Source. **P*<0.05; ***P*<0.01; ****P*<0.001; and *****P*<0.0001.

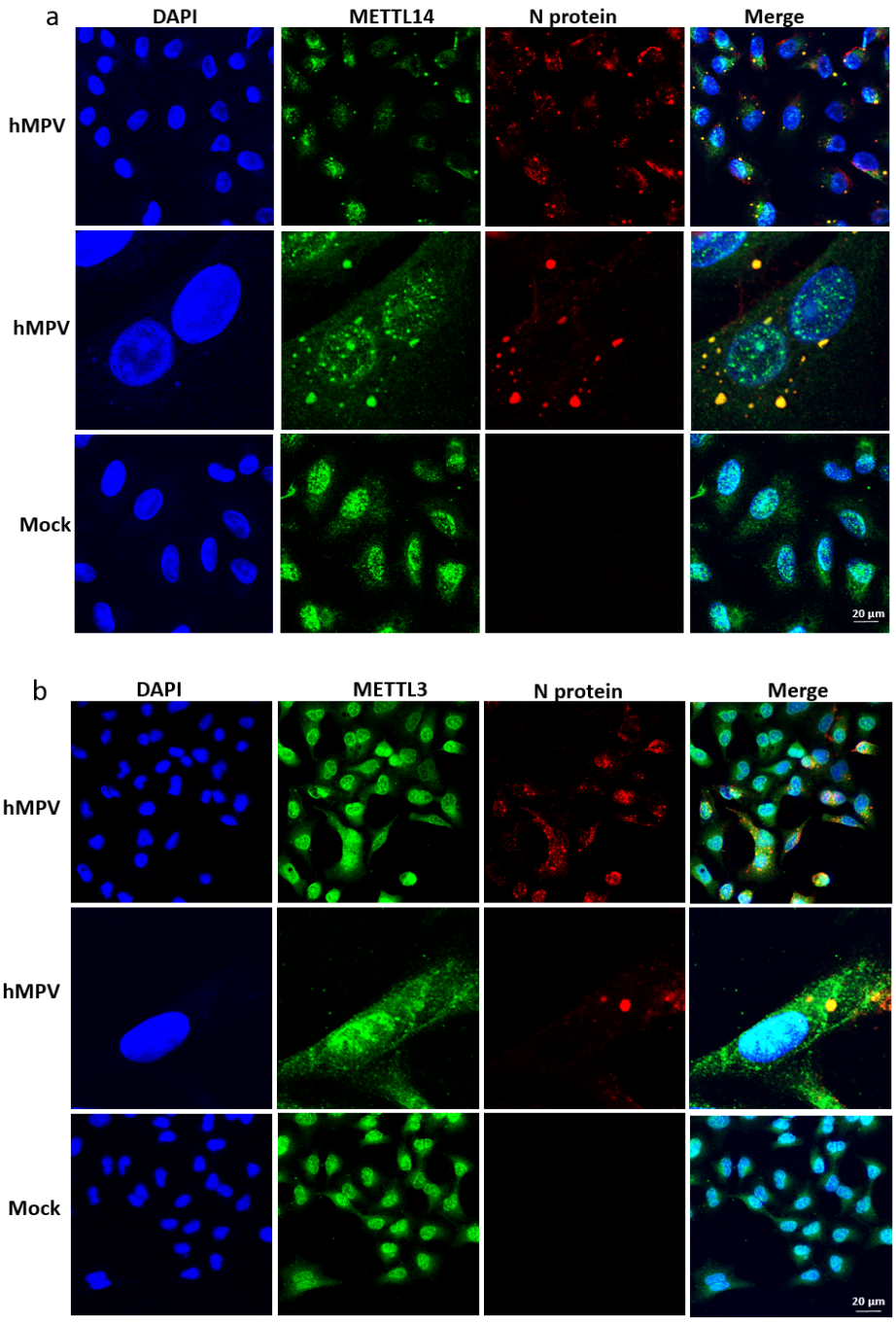

Supplementary Fig.2. The effects of hMPV infection on distribution of m^{6}A writer proteins in cells. A549 cells were infected by rhMPV at an MOI of 5.0. At 24 h post-infection, mock- or rhMPV-infected cells were stained with writer protein antibody (green) and anti-hMPV N protein antibody (red), and were analyzed by confocal microscope. Nuclei were labeled with DAPI (blue). **(a)** METTL14; **(b)** METTL3. Representative results from n = 3 biologically independent experiments are shown.

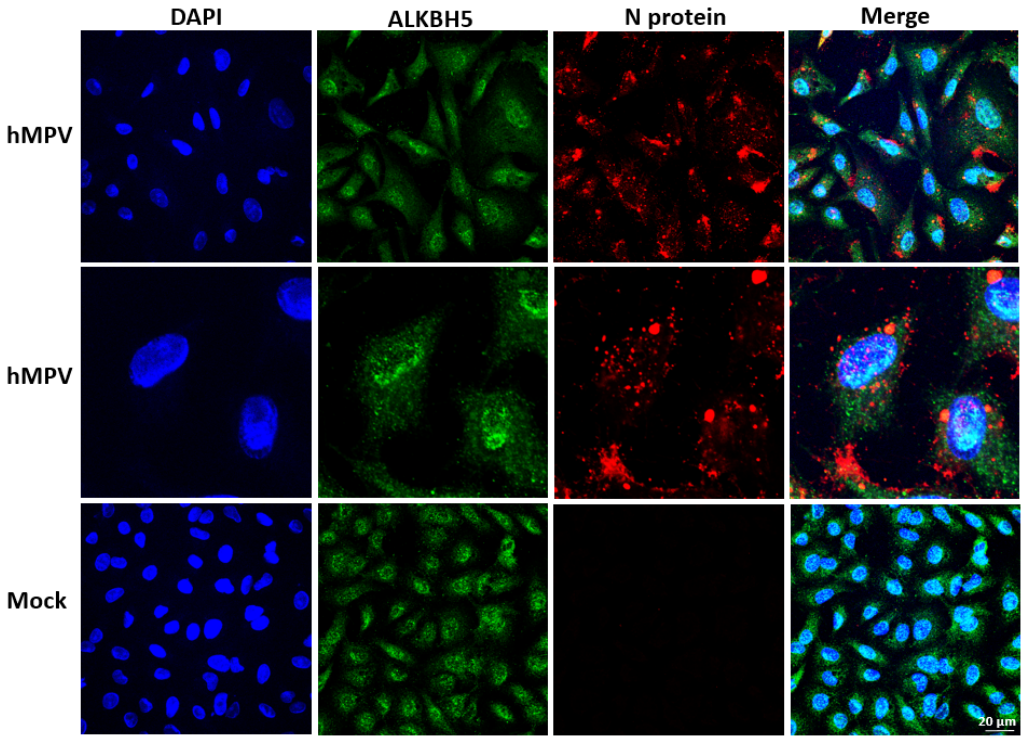

Supplementary Fig.3. The effects of hMPV infection on distribution of m^{6}A eraser proteins in cells. A549 cells were infected by rhMPV at an MOI of 5.0. At 24 h post-infection, mock- or rhMPV-infected cells were stained with anti-ALKBH5 antibody (green) and anti-hMPV N protein antibody (red), and were analyzed by confocal microscope. Nuclei were labeled with DAPI (blue). Representative results from $n = 3$ biologically independent experiments are shown.

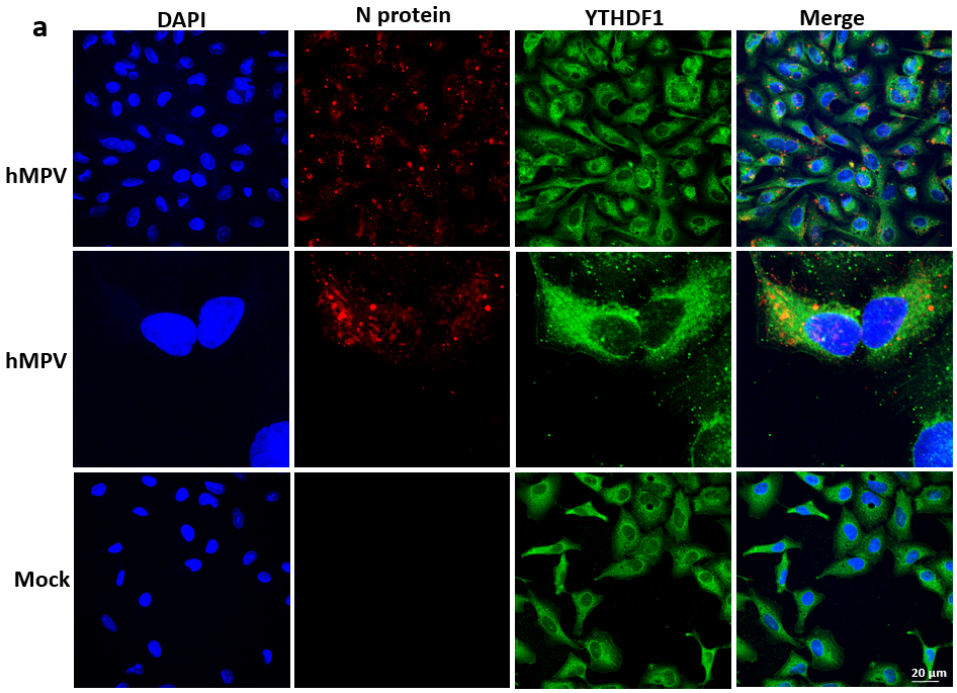
a
DAPI
N protein
YTHDF1
Merge
hMPV
hMPV
Mock
20 μm

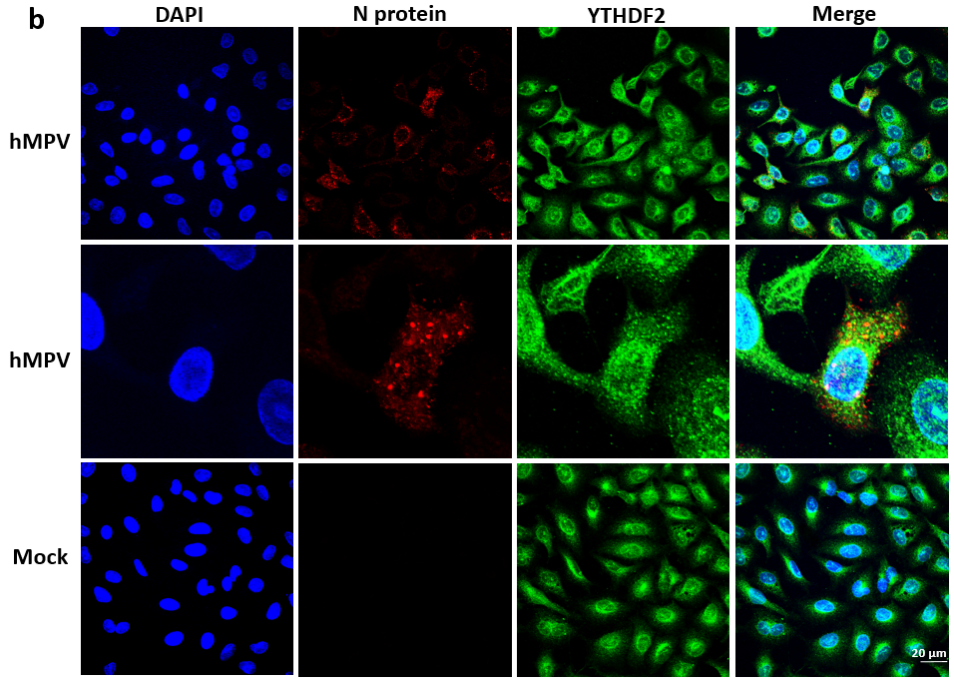
b
DAPI
N protein
YTHDF2
Merge
hMPV
hMPV
Mock
20 μm

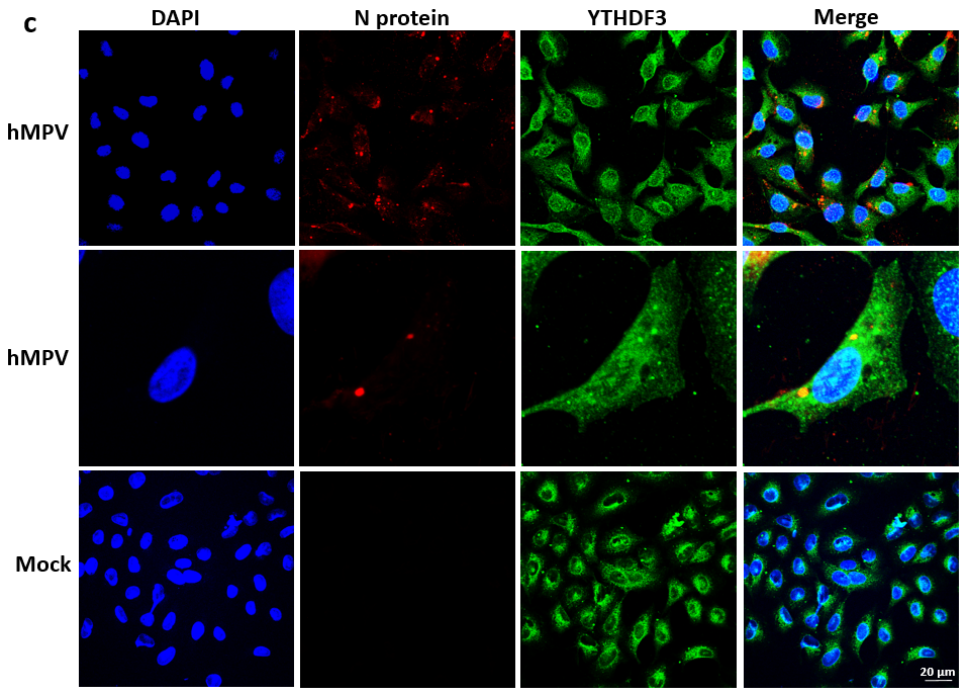

Supplementary Fig.4. Distribution of m^{6}A reader proteins in mock and hMPV-infected A549 cells. A549 cells were infected with rhMPV at an MOI of 5.0. At 24 h post-infection, mock- or rhMPV-infected cells were stained with anti-reader antibody (green) and anti-hMPV N protein antibody (red), and analyzed by confocal microscopy. Nuclei (blue) were labeled with DAPI. **(a) YTHDF1; (b) YTHDF2; and (c) YTHDF3.** Representative results from n = 3 biologically independent experiments are shown.

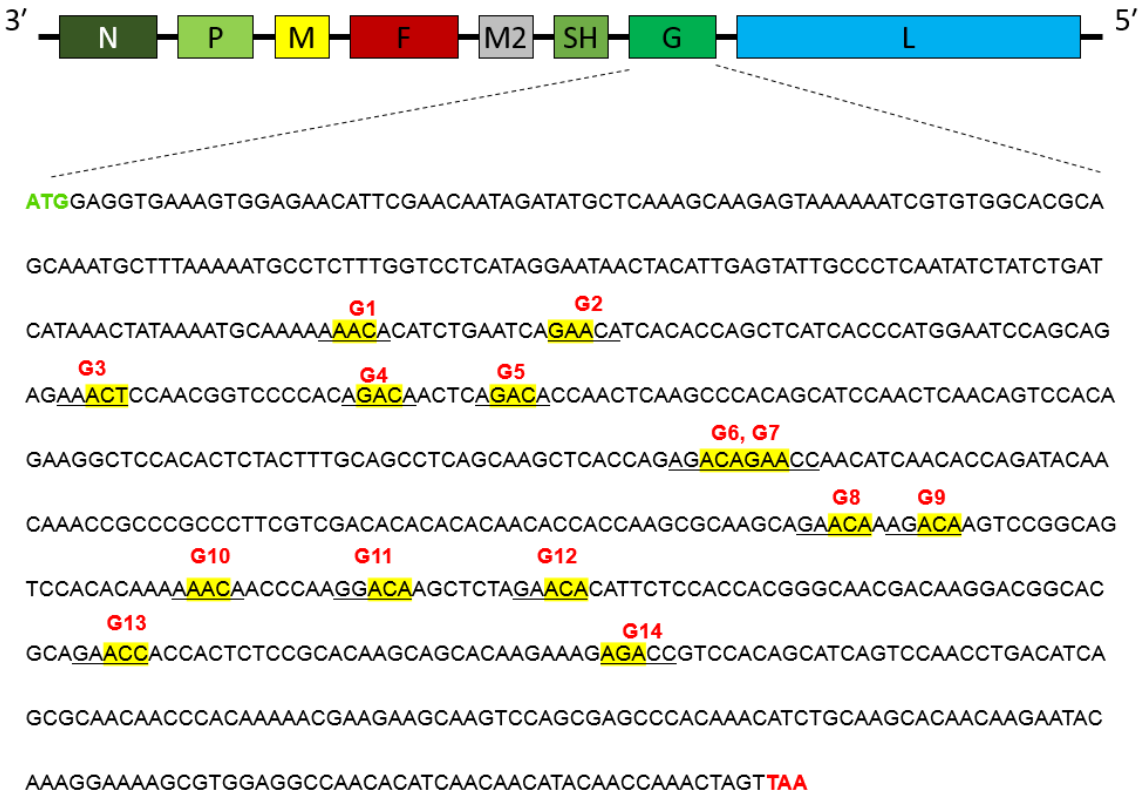

Supplementary Fig.5. Mutagenesis strategy in putative m^{6}A site in the G gene region in hMPV antigenome and mRNA. Schematic diagram of the hMPV genome with the mutations for altering the critical A or C residues in the m^{6}A motifs to produce rhMPV lacking that putative m^{6}A modification site in the G gene. A total of 14 putative m^{6}A site, G1-G14, are shown. G gene sequence of hMPV strain (subtype A strain NL/1/00, GenBank accession number AF371337) is shown.

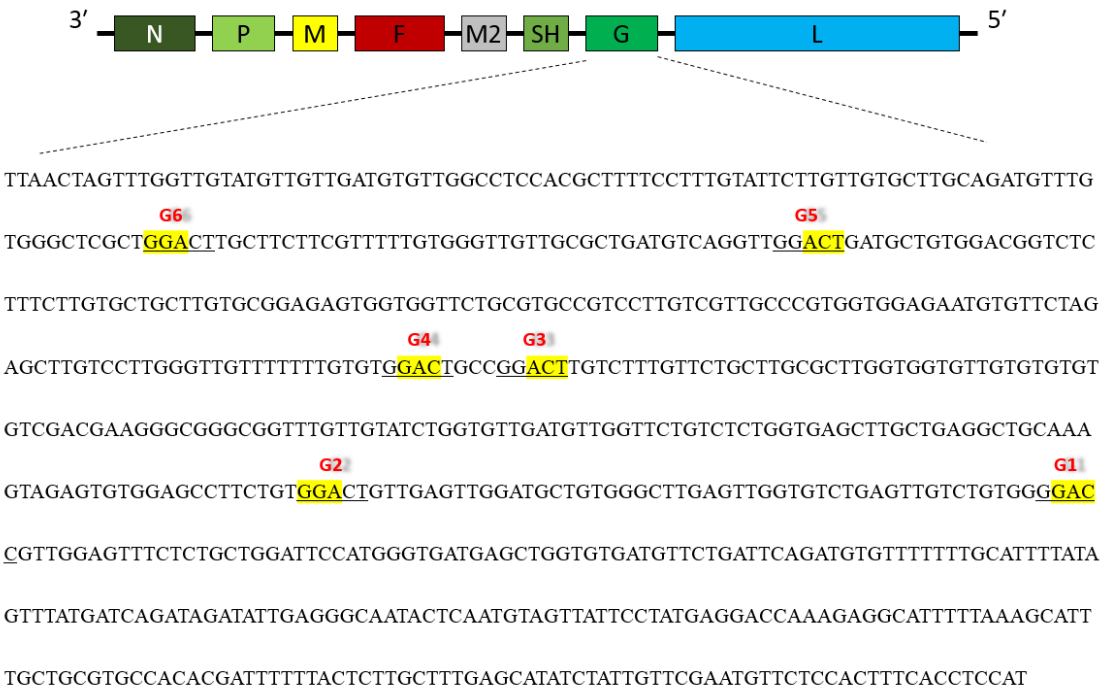

Supplementary Fig.6. Mutagenesis strategy in putative m^{6}A site in the G gene in hMPV genome. Schematic diagram of the hMPV genome with the mutations for altering the critical A or C residues in the m^{6}A motifs to produce rhMPV lacking that putative m^{6}A modification site in the G gene. A total of 6 putative m^{6}A site, G1-G6, are shown.

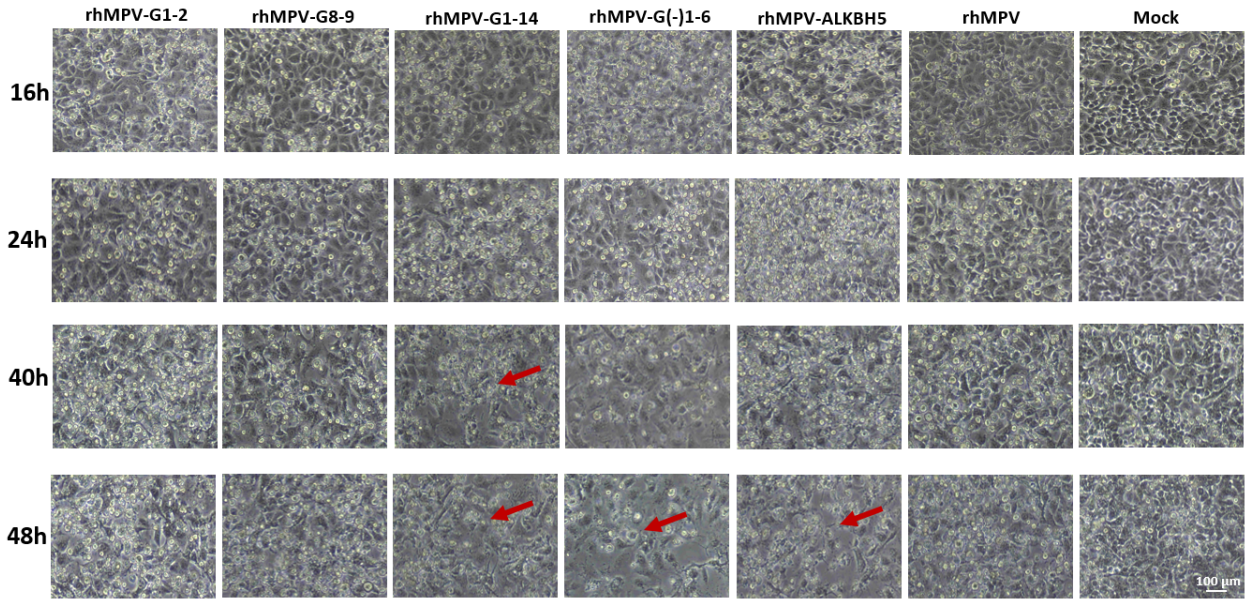

Supplementary Fig.7. CPE produced by m^{6}A-deficient hMPVs in A549 cells. Confluent A549 cells in 24-well plates were infected by each rhMPV mutant at an MOI of 5.0. CPE was imaged at 16, 24, 40 and 48 h post-infection. Red arrow indicates CPE. Representative images from n = 3 biologically independent experiments are shown.

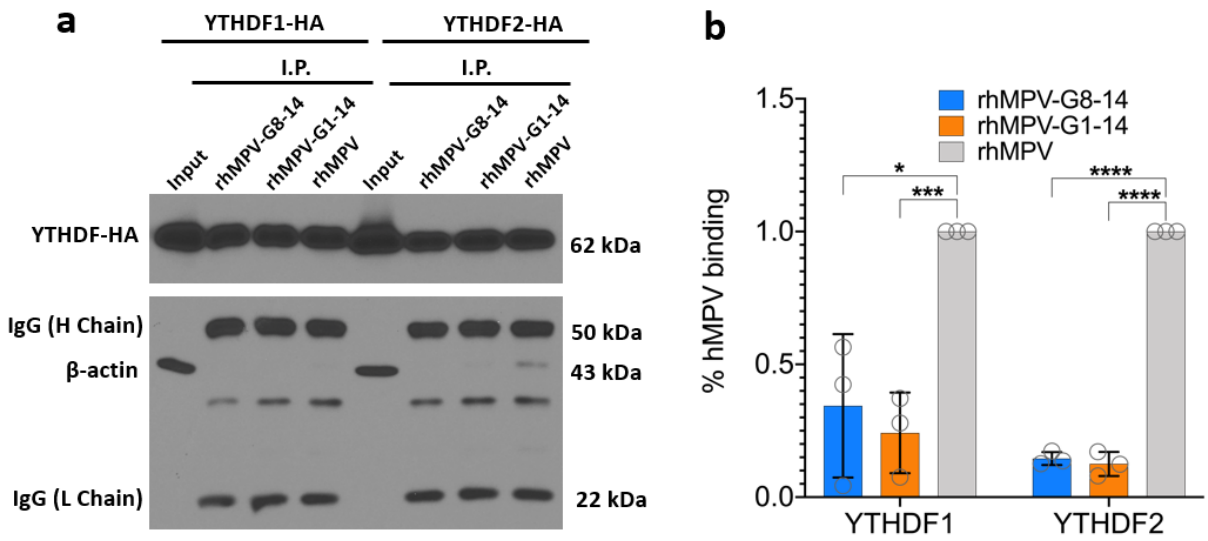

Supplementary Fig.8. m^{6}A-deficient rhMPV RNA has reduced binding efficiency to reader proteins. A549 cells in T25 flasks were transfected with plasmid pYTHDF1-HA or pYTHDF2-HA, and were lysed in 650 µL 1× lysis buffer (abcam, ab152163) at 24 h post transfection. Cell lysate was divided into 3 tube (200 µL/tube) and incubated with 2×10^8 copies of virion RNA (rhMPV-G8-14, rhMPV-G1-14, or rhMPV) and then incubated with 50µL Pierce anti-HA Magnetic beads at room temperature for 30 min. Reader protein: RNA complex pulled down by the beads was subjected to Western blot **(a)**. The amount of virion RNA captured by the YTHDF1 or YTHDF2 was quantified by real-time RT-PCR. Percent of bound RNA of hMPV mutants relative to rhMPV was calculated **(b)**. Input equals to 5µL of original lysate, and each I.P. sample equals to 40µL of original lysate. Western blots (**a**) shown are the representatives of n = 3 biologically independent experiments. Data shown (**b**) are averages of n =3 biologically independent experiments ± standard deviation. Statistical significance was determined by two-sided student's t-test. P values of rhMPV-G8-14 or rhMPV-G1-14 compared to rhMPV are as follows: YTHDF1, *P=0.01361, ***P=0.00099; YTHDF2, ****P=0.0000005, ****P=0.000005.

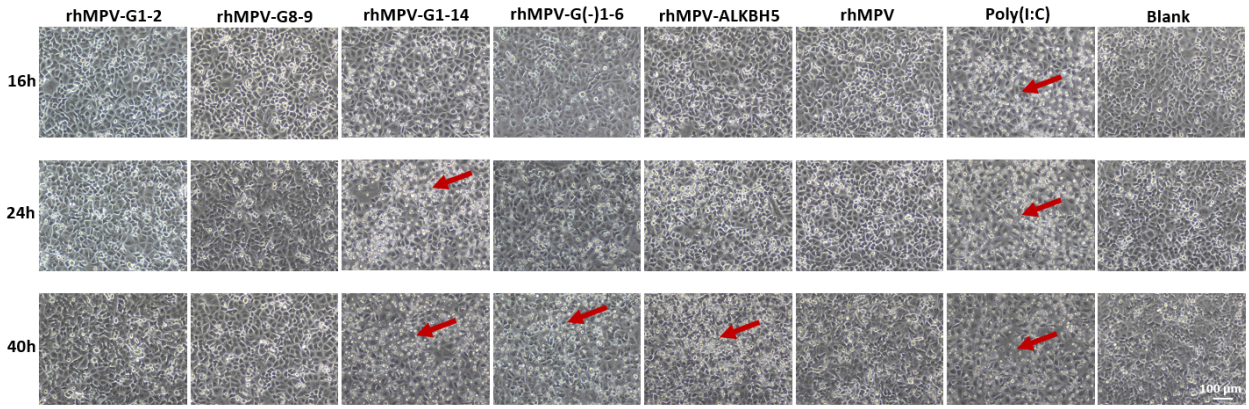

Supplementary Fig.9. Cell-death triggered by virion RNA of m^{6}A-deficient hMPVs. Virion RNA was extracted from purified hMPV virions, the level of antigenome was quantified by real-time RT-PCR. A549 cells in 24-well plates were transfected with 2×10^7 antigenome copies of virion RNA of each hMPV. Images were taken at 16, 24, and 40 post-transfection. Red arrow indicates CPE. Representative images from n = 3 biologically independent experiments are shown.

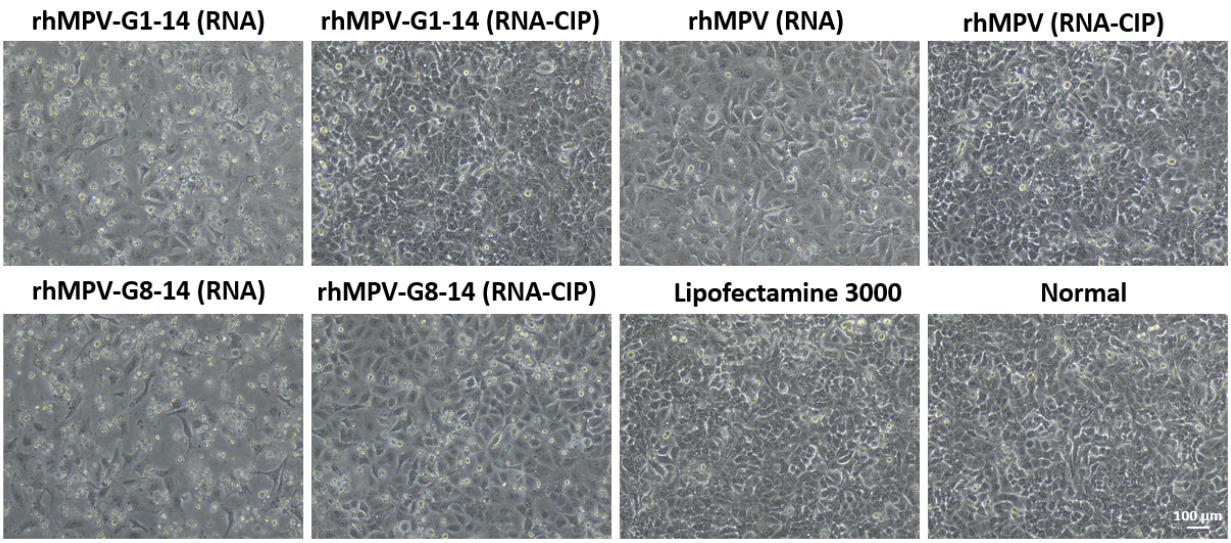

Supplementary Fig.10. Cell-death triggered by virion RNA of m^{6}A-deficient hMPVs with or without CIP. Virion RNA was extracted from purified hMPV virions, the level of antigenome was quantified by real-time RT-PCR. A549 cells in 24-well plates were transfected with 2×10^7 antigenome copies of virion RNA of each hMPV either with or without CIP treatment. Images were taken at 48 post-transfection. Representative images from n = 3 biologically independent experiments are shown.

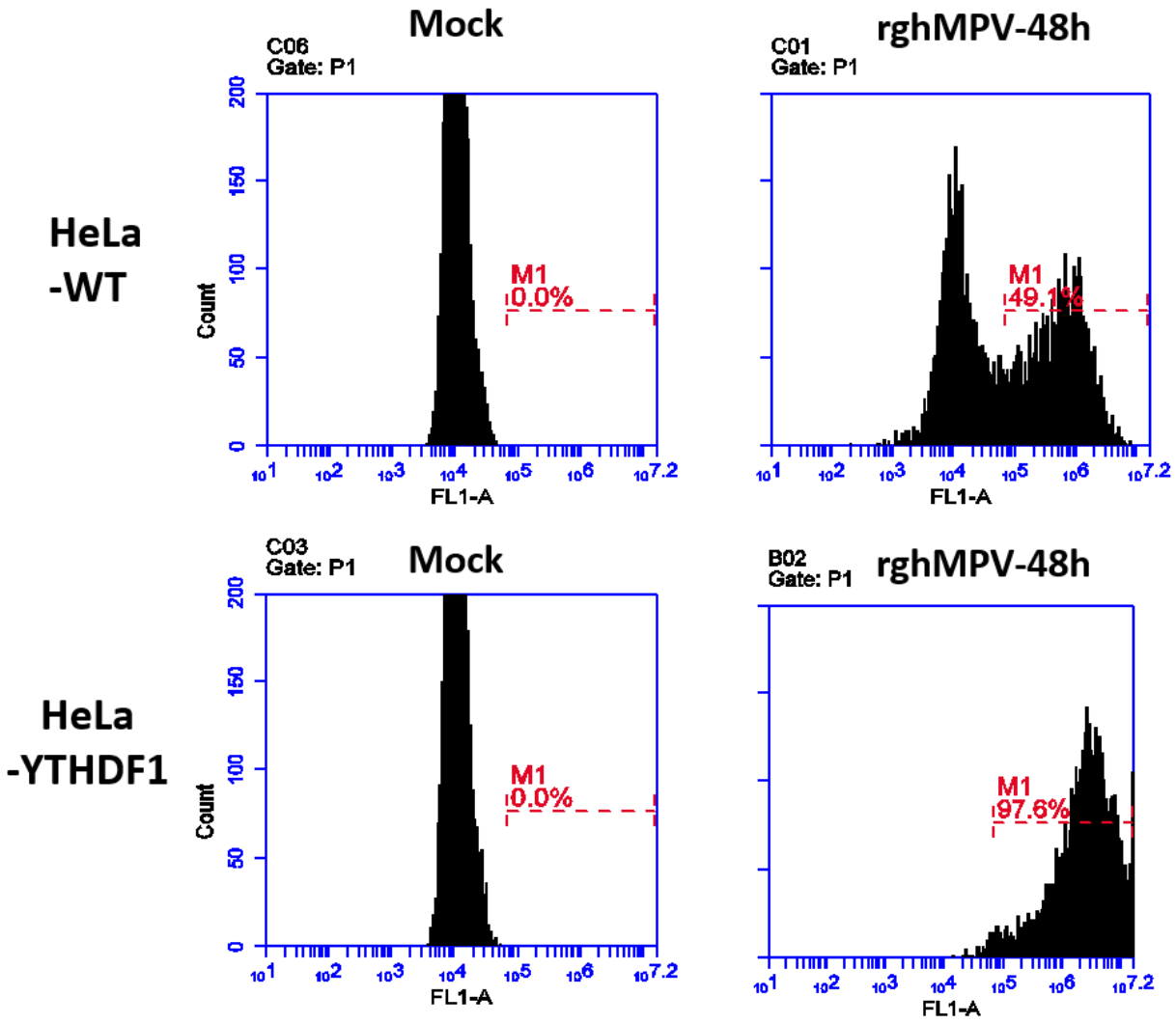

Supplementary Fig.11. An example of gating strategy for flow cytometry. WT HeLa cells or HeLa cells stably overexpressing YTHDF1 were infected with rghMPV at an MOI of 1.0. At 48 h post-inoculation, cells were trypsinized and fixed in 4 % of paraformaldehyde and the number of GFP-positive cells quantified by flow cytometry using Attune NxT Flow Cytometer. The mock-infected cells (left panel) were used for gating controls. Then, the number of GFP-positive and negative cells in rghMPV-infected cells were sorted (right panel). Attune NxT software was used to collect and analyze the data. The results showed that 49.1% and 97.6% cells are GFP-positive in rghMPV-infected HeLa-WT and HeLa-YTHDF1 cells respectively. The data shown are the representatives from $n = 3$ biologically independent experiments.

Supplementary Table 1: List of m^{6}A peaks in hMPV genome, antigenome, and mRNAs.

hMPV RNAs	Peak no.	Peak range (nt) [a]	*P* value	Gene location [b]	Peak size (nt)	Enrichment Fold [c]
Genome	1	1498-1617	7.23×10^{-10}	P	119	1.59
	2	1887-1916	2.23×10^{-8}	P	29	2.15
	3	2097-2126	2.26×10^{-4}	P	29	2.33
	4	6499-6558	4.53×10^{-68}	G	59	3.06
	5	6649-6947	1.0×10^{-128}	G	298	2.79
Antigenome	1	241-389	4.47×10^{-127}	N	148	2.35
	2	420-449	2.10×10^{-2}	N	29	1.16
	3	1468-1587	1.0×10^{-128}	P	119	3.12
	4	1768-1916	1.0×10^{-128}	P	148	2.96
	5	2816-2935	4.47×10^{-65}	M	119	1.86
	6	3265-3294	9.62×10^{-13}	F	29	2.05
	7	3325-3414	2.58×10^{-75}	F	89	2.42
	8	3534-3623	2.84×10^{-7}	F	89	1.36
	9	3954-4042	4.65×10^{-12}	F	88	1.53
	10	4373-4492	1.99×10^{-33}	F	119	1.96
	11	6404-6902	1.0×10^{-128}	G	498	3.12
	12	10691-10780	6.19×10^{-22}	L	89	2.08
mRNA	1	1513-1572	1.0×10^{-128}	P	59	1.78
	2	6459-6577	1.0×10^{-128}	G	118	12.31
	3	6637-6844	1.16×10^{-5}	G	207	14.808
	4	10735-10764	1.0×10^{-128}	L	29	1.22

a. Nucleotide sequence is referred to subtype A strain NL/1/00 (GenBank accession number AF371337). Nucleotide ranges are indicated. These regions contain putative m^{6}A sites. b. The hMPV genes are covered by m^{6}A peaks. c. Log enrichment of the m^{6}A peaks identified in hMPV antigenome, genome, and mRNA. Two replicates (n = 2) of RNA samples from virions, virus-infected cells, and mock-infected cells were subjected to m^{6}A-seq. For data analysis, after removing the adapter sequences, the reads were mapped to the human genome (hg38) and hMPV genome using Hisat2. Peak calling for the viral genome RNA was done by first dividing the hMPV genome into 30bp consecutive bins where read counts were quantified. Then we applied Fisher's exact test to assess the enrichment of coverage by m^{6}A-IP in these bins. The odds ratios were computed by (IP/overall IP)/(Input/overall Input) where overall IP/Input were represented by the median of read counts of bins across the same strand of the whole virus genome. Note, when calling peaks for mRNAs of the hMPV, the overall IP/Input were represented by the median of bins across the gene instead of the whole virus genome. Finally, we merged all neighboring bins that were significant (at FDR < 0.05 cutoff) in all replicates and reported them as consistent peaks. Statistical analysis was determined by Fisher's exact test. The *P* value for each peak is indicated.

Supplementary Table 2. Differentially m^{6}A methylated peaks in A549 cells after hMPV infection. The m^{6}A-methylome of the mock infected and hMPV infected cells was compared. Fisher's exact tests were used for peak calling. QNB package was used for differential methylation test with default setting. Two replicates (n = 2) of RNA samples from virus-infected cells and mock-infected cells was used for analysis. A total of 21 differentially m^{6}A methylated peaks are identified using count based QNB test.

Supplementary Table 3. **Differentially expressed genes in A549 cells after hMPV infection.** The input of m^{6}A-seq is equivalent to regular RNA-seq, therefore we quantified the gene-level read counts of input samples that aligned to hg38 for differential gene expression analysis. Wald test implemented in DESeq2 was used to make inferential tests where differentially expressed genes were identified at FDR < 0.1 cutoff. Two replicates (n = 2) of RNA samples from virus-infected cells and mock-infected cells was used for analysis. Over three thousand differentially expressed genes are identified by analysis of RNA-seq data of host cell (A549) at adjusted P value cutoff of 0.1.

Supplementary Table 4. List of upregulated genes involved in antiviral immune response after hMPV infection. Differentially expressed genes are identified using count based QNB test. Wald test implemented in DESeq2 were used. Two replicates (n = 2) of RNA samples from virus-infected cells and mock-infected cells were used for analysis. Numerous interferon encoded genes are upregulated including interferon lambda receptor 1, interferon beta 1, interferon lambda 2, interferon lambda 4, and genes involved in Pattern Recognition Receptor (PRR) including RIG-I, MDA5, LPG2, and multiple interferon-stimulated genes (ISGs).

Supplementary Table 5. List of siRNAs used for experiments.

siRNA	Sequences (5'-3')
YTHDF1	5'-CCGCGTCTAGTTGTTCATGAA-3'
YTHDF2	5'-AAGGACGTTCCCAATAGCCAA-3'
YTHDF3	5'-ATGGATTAAATCAGTATCTAA-3'
METTL3	5'-CTGCAAGTATGTTCACTATGA-3'
METTL14	5'-AAGGATGAGTTAATAGCTAAA-3'
ALKBH5	5'-AAACAAGTACTTCTTCGGCGA-3'
FTO	5'-AAATAGCCGCTGCTTGTGAGA-3'
Control siRNA	5' ACGTGACACGTTCGGAGAA-3'

Supplementary Discussion

Our RNA-seq found that highly purified hMPV virions contain both the genome and the antigenome. To confirm this, purified hMPV virions were disrupted by detergent, digested with RNase, and the RNase-resistant viral nucleocapsid (N-RNA complex) was pulled down by hMPV N antibody. Real-time RT-PCR analysis of nucleocapsid showed that the N-encapsidated genome and antigenome are indeed packaged into hMPV virions. Similarly, we recently showed that antigenome was packaged into virions of human respiratory syncytial virus (RSV) [1], another penumovirus. Also, studies in early 1970s found that antigenomes of several paramyxoviruses (such as Sendai virus and Newcastle disease virus) were packaged into mature virions [2, 3]. Interestingly, the amount of antigenome in mature virions is dependent on different virus strains and host cell lines [2]. In addition, the antigenomes of Sendai virus were shown to bud into virus particles as efficiently as the genomes [3].

Our main conclusion is that N^6-methyladenosine is a molecular signature for discriminating self from non-self RNA by RNA sensor RIG-I. A model consistent with our findings is depicted in **Fig.4i**. Upon virus entry, the ribonucleoprotein (RNP) complex, composed of the genome wrapped in the nucleocapsid (N) protein, associated with the viral RNA-dependent RNA polymerase (RdRP), is delivered into the cytoplasm where viral transcription and replication occur. During transcription, the RdRP sequentially transcribes the 8 viral genes into 9 mRNAs which are m^6A methylated and translated into 9 proteins, including the N protein. During replication, the RdRP initiates at the extreme 3' end of the genome and synthesizes a full-length complementary antigenome, which is methylated by m^6A writer proteins and

306 subsequently encapsidated by soluble N protein in a helical nucleocapsid with 9 to 10
307 bases/rotation of the helix [4]. This N-antigenomic RNA serves as template for synthesis of full-
308 length progeny genomes, which are also m^{6}A methylated and encapsidated by soluble N protein.
309 RNA m^{6}A methylation likely occurs prior to or concomitant with encapsidation, supported by
310 the observation that N is partially co-localizes with METTL3 and strongly co-localizes with
311 METTL14 in inclusion bodies where new RNP is assembled and active viral replication occurs.
312 The antigenome and genome are 5' triphosphorylated. Those that are not m^{6}A methylated are
313 recognized as a "nonself RNA" by RIG-I. The deficiency of m^{6}A in virion RNA induces higher
314 RIG-I expression, an enhanced RIG-I binding affinity and an enhanced ability to trigger the
315 conformational change in RIG-I that corresponds to enhanced signaling to the downstream
316 adaptor protein MAVS, activating IRF3 and NF-κB pathways, leading to higher production of
317 type-I IFN and proinflammatory cytokines. In contrast, although the wild type hMPV virion
318 RNA can be recognized by RIG-I due to the 5'ppp, the internal m^{6}A modification appears to
319 interfere with the high affinity binding of the RNA with the RIG-I helicase domain. Without this
320 separate RNA interaction, the low binding affinity association with 5'ppp does not appear to
321 efficiently induce the RIG-I mediated IFN signaling pathway. In addition, RIG-I is a 5'-
322 triphosphate-dependent translocase, traveling from the 5'-ppp into the RNA chain to trigger
323 oligomerization [5, 6]. Recently, it was found that the translocation of RIG-I and the following
324 RIG-I oligomerization is hindered by internal 2'-O methylation in dsRNA [7]. Thus, it is likely that
325 m^{6}A methylation may also serve as a "brake" or "throttle" to prevent RIG-I translocation and
326 oligomerization, leading to downstream signaling
327 .

One aspect of this scenario would seem to be unlikely, that the m^{6}A-modified genome or antigenome, tightly encapsidated by the N protein, would be accessible to RIG-I. And even if RIG-I could bind to the terminal 5'ppp, how would it be able to reach further into the RNA to find a non-methylated m^{6}A site? A more likely scenario might be that all of the genomes and antigenomes that are synthesized are not encapsidated. Particularly early in the infectious cycle, when the concentration of the N protein is low, some of these full-length RNA genomes and antigenomes may not be encapsidated, enabling RIG-I access to both the 5'ppp and RNA downstream from it. Unencapsidated full-length genome or antigenome RNAs would likely be fragile, as they are susceptible to cytoplasmic RNases. However, only a 5' fragment would be necessary to activate RIG-I in this scenario.

Our m^{6}A-seq analysis showed that all three species of viral RNA are m^{6}A methylated and the strongest m^{6}A peaks are located in the G gene mRNA and the region corresponding to the G gene in both genome and antigenome, leading us to mutate these m^{6}A sites. We modified the positive-strand RNA, disrupting m^{6}A sites of both the G mRNA (transcription product) and antigenome (replication intermediate). We also mutated the m^{6}A sites in the G gene in negative-sense genome RNA. By overexpressing m^{6}A eraser protein, we generated hMPV that is naturally defective in m^{6}A methylation in its antigenome and genome. In all cases, these m^{6}A-deficient rhMPVs and their virion RNAs induced significantly higher type I IFN responses. Both genome and antigenome ssRNAs contain 5' triphosphate, a known ligand for RIG-I [8, 9]. Removal of the 5' triphosphate abrogated the RIG-I expression, RIG-I binding, IRF3 phosphorylation, and IFN response of both wild type antigenome and m^{6}A-deficient antigenome, suggesting that 5' triphosphate is absolutely required for RIG-I signaling. However, when m^{6}A sites in the

antigenome and genome were mutated or naturally removed by eraser proteins, the expression of RIG-I and the binding affinity of RIG-I for the m^{6}A-deficient virion RNA was significantly enhanced compared to the wild type virion RNA, leading to a higher type I IFN response. Thus, marking antigenome and genome RNA with m^{6}A methylation allows it to escape detection by RIG-I. The m^{6}A sites in both genome and antigenome are involved in innate immune recognition.

The crystal structures of the ligand-free, autorepressed, and RNA-bound, activated states of RIG-I has been resolved [10, 11, 12]. These structure studies provided a detailed view of how RIG-I recognizes the 5'end of double strand RNA (dsRNA) or single strand RNA (ssRNA) and how RIG-I conformational change occurs upon binding to these short RNA ligands. Based on these structure studies, a limited trypsin digestion assay is developed and often used for discriminating the autorepressed and the activated states of RIG-I [10, 13, 14]. It should be noted that these structural and biochemical studies used in vitro synthesized, short ssRNA or dsRNA as the RNA ligand. In this study, we compared the trypsin sensitivity of RIG-I upon binding of full-length hMPV genome and antigenome RNA (13,350 bp), virion RNA of rhMPV-G1-14 and G8-14 yielded significantly more trypsin-resistant 80-kDa fragment than RNA of rhMPV-G1-2, G8-9, and rhMPV. These results demonstrated that m^{6}A-deficient virion RNA facilitates RIG-I conformational changes and forms RIG-I: RNA complex which is more resistant to trypsin digestion. However, it is unclear whether this assay really represent how native viral RNA interacts with RIG-I. A future direction is to determinate the structure of RIG-I with m^{6}A sufficient or m^{6}A-deficient antigenome and genome RNA.

373 It is unlikely that the defective interfering (DI) particles contribute to the higher
374 activation of RIG-I in our experiments. We used a relatively low MOI (0.5) for preparation of
375 virus stock. All virus stocks were purified through a sucrose gradient ultracentrifugation, which
376 allows for separation of infectious virus particles and DI particles. Solution layer containing
377 virus was extracted with syringe to avoid any possible contamination of DI particles. Our RNA
378 transfection experiment showed that the degrees of defects in virion RNA m^6A methylation were
379 nicely correlated with the levels of type I IFN responses and the levels of signaling molecules
380 involved in the RIG-I mediated IFN pathway. Our finding was further supported by the rhMPV-
381 ALKBH5, a recombinant hMPV that is naturally defective in m^6A methylation in genome and
382 antigenome.
383
384 Unlike genome and antigenome, hMPV mRNAs are capped and G-N-7 and ribose 2'-O
385 are methylated at the 5' end and the mRNA is polyadenylated at the 3' end. Neither modification
386 is recognized by RIG-I or MDA5. Previously, it was shown that viral mRNA lacking 2'-O
387 methylation can be detected by MDA5 and the IFIT family, highlighting that 2'-O methylation
388 also serves as a molecular marker for host innate immunity to discriminate self from nonself
389 mRNA. Here we found that m^6A deficient G mRNA with G-N-7 and ribose 2'-O methylation is
390 not recognized by RIG-I or MDA5, suggesting that m^6A methylation in mRNA does not play a
391 role in innate immunity. However, our data suggest that m^6A methylation of viral mRNA plays
392 an important role in enhancing mRNA translation. First, overexpression of m^6A reader and
393 writer proteins enhanced G protein expression whereas knockdown of these proteins inhibited G
394 expression. Second, G protein expression was inhibited when m^6A sites in G mRNA were
395 mutated. The impact of m^6A methylation on mRNA stability and protein synthesis is relatively

well understood. For example, METTL3 knockdown caused nearly 30% decrease of global protein synthesis [15]. All three m^{6}A reader proteins can promote translation of host and viral protein translation. In addition, YTHDF2 can regulate decay of both host and viral mRNAs [16, 17]. YTHDF2 can bind to m^{6}A-methylated transcripts leading to its re-localization from the pool of ribosome-associated translatable transcripts to the P-bodies where RNA decay occurs [16].

Notably, we found that m^{6}A-deficient hMPVs triggered significantly higher type I interferon responses compared to the parental hMPV, thereby contributing to the restriction of viral replication. In addition, both m^{6}A-deficient rhMPV and isolated antigenome and/or genome RNA induced higher expression of RIG-I. However, IFN response was completely abrogated when RIG-I or MAVs but not MDA5 were knocked out from A549 cells. The binding affinity of RIG-I to m^{6}A-deficient RNAs significantly increased compared to the m^{6}A-sufficient RNAs. This suggests that RIG-I played a dominant role in recognizing m^{6}A-deficient rhMPV and antigenome. This conclusion was further supported by the fact that the replication of m^{6}A-deficient hMPVs was completely or partially restored in A549 cells when RIG-I or MAVs but not MDA5 were knocked out. In addition, we found that m^{6}A-deficient rhMPV and antigenome triggered a higher NF-κB driven SEAP activity. These results suggest that m^{6}A-deficient RNA contributes to the enhanced activation of transcription factors belonging to the NF-κB and IRF families which lead to the enhanced expression of IFN. On the other hand, recent evidence suggests that m^{6}A writer and eraser proteins are involved in regulation of innate immune responses by affecting export, stability, and translation of antiviral genes [18, 19]. For example, upon VSV infection, DEAD-box helicase (DDX46) was shown to recruit m^{6}A eraser protein ALKBH5 to demethylate m^{6}A-modified antiviral transcripts, resulting in retention of these

419 transcripts in the nucleus, prevention of their translation, and inhibition of interferon production
420 and antiviral responses [19]. Depleting METTL14 increased both nascent IFNB1 mRNA
421 production and stability in response to dsDNA or human cytomegalovirus (HCMV) infection [18].
422 In contrast, ALKBH5 depletion had the opposite effect [18]. In a separate study, it was shown that
423 IFNB mRNA is m^{6}A modified and is more stable in METTL3- and YTHDF2-depleted cells,
424 leading to an increase in IFN production following HCMV infection [20].
425
426 Overall, the degrees of the defects in RNA m^{6}A methylation are highly correlated with the
427 levels of type I IFN responses and the levels of signaling molecules involved in the RIG-I
428 mediated pathway. Antigenome of rhMPV-G1-14 contains more m^{6}A site mutations than the
429 antigenome of rhMPV-G1-2 and G8-9. Consistent with higher defects in m^{6}A methylation, the
430 antigenome of rhMPV-G1-14 induced significantly higher RIG-I expression, more RIG-I
431 conformational changes, and more IFN production than the antigenome of rhMPV-G1-2 and G8-
432 9 when their virion RNAs were transfected into A549 cells. Interestingly, in virus-infected cells,
433 rhMPV-G1-2 and G8-9 induced more IFN than rhMPV-G1-14 under some conditions (e.g. MOI
434 of 4.0 in A549 cells). We interpret this discrepancy as being due to the complicated nature of
435 IFN regulation during hMPV infection, involving viral RNA replication, protein synthesis, and
436 alteration of host gene expression. In contrast, virion RNA transfection avoids these
437 complicating factors, examining more directly the effects of m^{6}A methylation of RNA on IFN
438 production. Importantly, in addition to the RIG-I pathway, several other signaling pathways
439 including MDA5 and TLR3/TLR4/TLR7 are triggered during hMPV infection [21, 22] and may play
440 a role. Also, several viral proteins (G, M2-2, SH, and P) have been shown to inhibit these
441 pathways [21, 22]. For example, it was shown that hMPV G protein inhibits innate immunity by
442 inhibiting RIG-I activation and impairing the TLR4-dependent signaling pathway [23, 24], based on

443 the observation that rhMPV lacking its G protein (rhMPV-ΔG) induced significantly higher
444 production of type I IFN and chemokines than wild type hMPV in A549 cells [23]. In fact, rhMPV-
445 ΔG was highly attenuated in viral replication in cell culture as well as in the upper and lower
446 respiratory tract of Syrian hamsters and African green monkeys [25]. Since the G gene region has
447 the strongest m^{6}A peaks in the hMPV genome, deletion of the G gene from the genome would
448 result in a natural m^{6}A-deficient virus. Thus, it is possible that m^{6}A-deficient genome and
449 antigenome produced by rhMPV-ΔG activated the RIG-I signaling pathway, rather than the loss
450 of G protein expression suppressing RIG-I. Purified virion RNA from m^{6}A deficient rhMPVs,
451 which did not contain any viral proteins, directly triggered higher RIG-I expression and a more
452 robust IFN response. In addition, compensation for the reduced G protein expression did not
453 inhibit the IFN response of these m^{6}A-deficient rhMPVs.
454
455 Viral RNA m^{6}A methylation and its functions is an emerging field that has only been
456 explored over the past two years. Detailed mechanisms by which m^{6}A controls virus replication
457 and gene expression are still poorly understood. We demonstrated that the multiple biological
458 functions of m^{6}A methylation collectively contribute to enhanced hMPV replication and gene
459 expression. First, during replication, the newly synthesized genome and replicative intermediate
460 (antigenome) are m^{6}A methylated by m^{6}A writer proteins to prevent their detection by the innate
461 immune system. Second, during transcription, viral mRNAs are also m^{6}A methylated which
462 enhances their translation which in turn may enhance virus spread. However, viral m^{6}A appears
463 to play an antiviral role in several flaviviruses such as HCV and Zika virus via an unknown
464 mechanism(s) [26, 27]. Resolving why m^{6}A has a pro-viral function in some viruses whereas it has
465 an antiviral function in other viruses may facilitate a strategy to develop m^{6}A as an antiviral drug

target.

One important application of this work is in the development of live attenuated vaccine candidates for hMPV by reducing m^{6}A methylation in viral RNAs. Currently, hMPV is the second leading causative agent of acute respiratory disease in infants, children, and the elderly [28, 29], behind RSV. Despite major efforts, there is no FDA-approved vaccine for hMPV [29]. Inactivated vaccines are not suitable for hMPV because they cause enhanced lung damage upon re-infection with the same virus [30]. In contrast, enhanced lung damage has not been observed for live attenuated vaccine candidates [31, 32]. Thus, a live attenuated vaccine is one of the most promising candidates for hMPV [33]. However, it has been a challenge to identify a live attenuated vaccine strain that has an optimal balance between attenuation and immunogenicity. Since viral m^{6}A acts in a pro-viral manner for hMPV, it should be feasible to generate an m^{6}A-deficient rhMPV strain that is sufficiently attenuated yet retains high immunogenicity. In this study, we showed that depletion of m^{6}A sites in G mRNA resulted in a recombinant virus (rhMPV-G1-14) that is sufficiently attenuated in replication in the lungs but only had a mild defect in replication in nasal turbinate. Cotton rats immunized with this m^{6}A-deficient hMPV expressed a high level of neutralizing antibody and were completely protected against challenge with parental rhMPV, highlighting the potential of utilizing an m^{6}A-deficient hMPV mutant as a live vaccine candidate. This phenotype is similar to that of the cold-adapted attenuated viruses, which replicate in upper but not lower respiratory tracts. Cold-adapted (*ca*) temperature sensitive (*ts*) influenza virus vaccine has been licensed for use in humans since 1980 [34, 35].

A distinct advantage of targeting m^{6}A sites for virus attenuation is that m^{6}A-deficient hMPV mutants are capable of inducing a significantly higher type I IFN response compared to rhMPV. A higher IFN response will likely enhance adaptive immunity. Targeting different combinations of the many viral m^{6}A sites could identify combinations with the optimal balance between attenuation and immunogenicity. A virus with mutations in multiple m^{6}A sites would have enhanced genetic stability because reversion at any one site would have only a minor fitness gain. In fact, all m^{6}A-deficient hMPV mutants were genetically stable; with no revertants or additional mutations detected after fifteen passages in A549 cells. In addition, m^{6}A-deficient hMPV mutants grew to reasonably high titers in cell culture, especially in IFN-deficient cells, making vaccine production economically feasible. Thus, inhibition of viral m^{6}A methylation is a novel approach to attenuating hMPV for the rational design of live attenuated vaccines.

In summary, we discovered that the presence of m^{6}A in virion RNA serves as a molecular signature for discrimination of self from non-self RNA by the cytoplasmic RNA sensor RIG-I. This work highlights that possibility of using m^{6}A as a novel approach for the development of antiviral drugs and live attenuated vaccines for pneumoviruses.

References

1. Xue, M. *et al.* Viral N(6)-methyladenosine upregulates replication and pathogenesis of human respiratory syncytial virus. *Nat. Commun.* **10**, 4595 (2019).
2. Kolakofsky, D. & Bruschi, A. Antigenomes in Sendai virions and Sendai virus-infected cells. *Virology* **66**, 185-191 (1975).
3. Mottet, G. & Roux, L. Budding efficiency of Sendai virus nucleocapsids: influence of size and ends of the RNA. *Virus Res.* **14**, 175-187 (1989).
4. Green, T.J., Zhang, X., Wertz, G.W. & Luo, M. Structure of the vesicular stomatitis virus nucleoprotein-RNA complex. *Science* **313**, 357-360 (2006).

5. Myong, S. *et al.* Cytosolic viral sensor RIG-I is a 5'-triphosphate-dependent translocase on double-stranded RNA. *Science* **323**, 1070-1074 (2009).
6. Zheng, J. *et al.* HDX-MS reveals dysregulated checkpoints that compromise discrimination against self RNA during RIG-I mediated autoimmunity. *Nat. commun.* **9**, 5366 (2018).
7. Devarkar, S.C., Schweibenz, B., Wang, C., Marcotrigiano, J. & Patel, S.S. RIG-I Uses an ATPase-Powered Translocation-Throttling Mechanism for Kinetic Proofreading of RNAs and Oligomerization. *Molecular Cell* **72**, 355-368 e354 (2018).
8. Hornung, V. *et al.* 5'-Triphosphate RNA is the ligand for RIG-I. *Science* **314**, 994-997 (2006).
9. Hyde, J.L. & Diamond, M.S. Innate immune restriction and antagonism of viral RNA lacking 2-O methylation. *Virology* **479-480**, 66-74 (2015).
10. Jiang, F. *et al.* Structural basis of RNA recognition and activation by innate immune receptor RIG-I. *Nature* **479**, 423-427 (2011).
11. Kowalinski, E. *et al.* Structural basis for the activation of innate immune pattern-recognition receptor RIG-I by viral RNA. *Cell* **147**, 423-435 (2011).
12. Luo, D. *et al.* Structural insights into RNA recognition by RIG-I. *Cell* **147**, 409-422 (2011).
13. Beckham, S.A. *et al.* Conformational rearrangements of RIG-I receptor on formation of a multiprotein:dsRNA assembly. *Nucleic Acids Res* **41**, 3436-3445 (2013).
14. Durbin, A.F., Wang, C., Marcotrigiano, J. & Gehrke, L. RNAs Containing Modified Nucleotides Fail To Trigger RIG-I Conformational Changes for Innate Immune Signaling. *MBio* **7** (2016).
15. Coots, R.A. *et al.* m(6)A Facilitates eIF4F-Independent mRNA Translation. *Molecular Cell* **68**, 504-514 e507 (2017).
16. Wang, X. *et al.* N6-methyladenosine-dependent regulation of messenger RNA stability. *Nature* **505**, 117-120 (2014).
17. Tan, B. *et al.* Viral and cellular N(6)-methyladenosine and N(6),2'-O-dimethyladenosine epitranscriptomes in the KSHV life cycle. *Nat. Microbiol.* **3**, 108-120 (2018).
18. Rubio, R.M., Depledge, D.P., Bianco, C., Thompson, L. & Mohr, I. RNA m(6) A modification enzymes shape innate responses to DNA by regulating interferon beta. *Genes & Development* **32**, 1472-1484 (2018).
19. Zheng, Q., Hou, J., Zhou, Y., Li, Z. & Cao, X. The RNA helicase DDX46 inhibits innate immunity by entrapping m(6)A-demethylated antiviral transcripts in the nucleus. *Nat. Immunol.* **18**, 1094-1103 (2017).
20. Winkler, R. *et al.* m(6)A modification controls the innate immune response to infection by targeting type I interferons. *Nat. Immunol.* **20**, 173-182 (2019).
21. Kolli, D., Bao, X. & Casola, A. Human metapneumovirus antagonism of innate immune responses. *Viruses* **4**, 3551-3571 (2012).
22. Cespedes, P.F., Palavecino, C.E., Kalergis, A.M. & Bueno, S.M. Modulation of Host Immunity by the Human Metapneumovirus. *Clin. Microbiol. Rev.* **29**, 795-818 (2016).
23. Bao, X. *et al.* Human metapneumovirus glycoprotein G inhibits innate immune responses. *PLoS Pathogens* **4**, e1000077 (2008).
24. Kolli, D. *et al.* Human metapneumovirus glycoprotein G inhibits TLR4-dependent signaling in monocyte-derived dendritic cells. *J. Immunol.* **187**, 47-54 (2011).

25. Biacchesi, S. *et al.* Recombinant human Metapneumovirus lacking the small hydrophobic SH and/or attachment G glycoprotein: deletion of G yields a promising vaccine candidate. *J. Virol.* **78**, 12877-12887 (2004).
26. Gokhale, N.S. *et al.* N6-Methyladenosine in Flaviviridae Viral RNA Genomes Regulates Infection. *Cell Host Microbe* **20**, 654-665 (2016).
27. Lichinchi, G. *et al.* Dynamics of Human and Viral RNA Methylation during Zika Virus Infection. *Cell Host & Microbe* **20**, 666-673 (2016).
28. van den Hoogen, B.G. *et al.* A newly discovered human pneumovirus isolated from young children with respiratory tract disease. *Nature medicine* **7**, 719-724 (2001).
29. Schildgen, V. *et al.* Human Metapneumovirus: lessons learned over the first decade. *Clin. Microbiol. Rev.* **24**, 734-754 (2011).
30. Yim, K.C. *et al.* Human metapneumovirus: enhanced pulmonary disease in cotton rats immunized with formalin-inactivated virus vaccine and challenged. *Vaccine* **25**, 5034-5040 (2007).
31. Zhang, Y. *et al.* Rational design of human metapneumovirus live attenuated vaccine candidates by inhibiting viral mRNA cap methyltransferase. *J. Virol.* **88**, 11411-11429 (2014).
32. Buchholz, U.J., Nagashima, K., Murphy, B.R. & Collins, P.L. Live vaccines for human metapneumovirus designed by reverse genetics. *Expert Review of Vaccines* **5**, 695-706 (2006).
33. Wen, S.C. & Williams, J.V. New Approaches for Immunization and Therapy against Human Metapneumovirus. *Clinical and Vaccine Immunology : CVI* **22**, 858-866 (2015).
34. Reeve, P., Almond, J.W., Felsenreich, V., Pibermann, M. & Maassab, H.F. Studies with a cold-recombinant A/Victoria/3/75 (H3N2) virus. I. biologic, genetic, and biochemical characterization. *J. Infect. Dis.* **142**, 850-856 (1980).
35. Murphy, B.R. *et al.* Cold-adapted variants of influenza A virus: evaluation in adult seronegative volunteers of A/Scotland/840/74 and A/Victoria/3/75 cold-adapted recombinants derived from the cold-adapted A/Ann Arbor/6/60 strain. *Infection and Immunity* **23**, 253-259 (1979).